MOLECULAR IMAGING AND BIOLOGY

Mol Imaging Biol (2021)
DOI: 10.1007/s11307-021-01603-2

WMIS World Molecular Imaging Society
esmi european society for molecular imaging

RESEARCH ARTICLE

Synthesis and Biological Evaluation of [^{18}F]FECNT-d_4 as a Novel PET Agent for Dopamine Transporter Imaging

Shanshan Cao,[1] Jie Tang,[2] Chunyi Liu,[2] Yi Fang,[2] Linyang Ji,[1] Yingjiao Xu,[2] Zhengping Chen[1,2]

[1]*Jiangsu Key Laboratory of New Drug Research and Clinical Pharmacy, School of Pharmacy, Xuzhou Medical University, Xuzhou, 221004, China*
[2]*NHC Key Laboratory of Nuclear Medicine, Jiangsu Key Laboratory of Molecular Nuclear Medicine, Jiangsu Institute of Nuclear Medicine, Wuxi, 214063, China*

Abstract

Purpose: The dopamine transporter (DAT) is a marker of the occurrence and development of Parkinson's disease (PD) and other diseases with nigrostriatal degeneration. 2β-Carbomethoxy-3β-(4-chlorophenyl)-8-(2-[^{18}F]-fluoroethyl)nortropane ([^{18}F]FECNT), an ^{18}F-labelled tropane derivative, was reported to be a useful positron-emitting probe for DAT. However, the rapid formation of brain-penetrating radioactive metabolites is an impediment to the proper quantitation of DAT in PET studies with [^{18}F]FECNT. Deuterium-substituted analogues have presented better *in vivo* stability to reduce metabolites. This study aimed to synthesize a deuterium-substituted DAT radiotracer, [^{18}F]FECNT-d_4, and to make a preliminary investigation of its properties as a DAT tracer *in vivo*.

Procedures: The ligand [^{18}F]FECNT-d_4 was obtained by one-step radiolabelling reaction. The lipophilicity was measured by the shake-flask method. Binding properties of [^{18}F]FECNT-d_4 were estimated by *in vitro* binding assay, biodistribution, and microPET imaging in rats. *In vivo* stability of [^{18}F]FECNT-d_4 was estimated by radio-HPLC.

Results: [^{18}F]FECNT-d_4 was synthesized at an average activity yield of 46 ± 17 % (n = 15) and the molar activity was 67 ± 12 GBq/μmol. The deuterated tracer showed suitable lipophilicity and the ability to penetrate the blood-brain barrier (brain uptake of 1.72 % ID at 5 min). [^{18}F]FECNT-d_4 displayed a high binding affinity for DAT comparable to that of [^{18}F]FECNT in rat striatum homogenates. Biodistribution results in normal rats showed that [^{18}F]FECNT-d_4 exhibited a higher ratio of the target to non-target (striatum/cerebellum) at 15 min post administration (5.00 ± 0.44 vs 3.84 ± 0.24 for [^{18}F]FECNT-d_4 vs [^{18}F]FECNT). MicroPET imaging studies of [^{18}F]FECNT-d_4 in normal rats showed that the ligand selectively localized to DAT-rich striatal regions and the accumulation could be blocked with DAT inhibitor. Furthermore, in the unilateral PD model rat, a significant reduction of the signal was found in the lesioned side relative to the unlesioned side. Striatal standardized uptake value of [^{18}F]FECNT-d_4 remained ~4.02 in the striatum between 5 and 20 min, whereas that of [^{18}F]FECNT fell rapidly from 4.11 to 2.95. Radio-HPLC analysis of the plasma demonstrated better *in vivo* stability of [^{18}F]FECNT-d_4 than [^{18}F]FECNT.

Conclusion: The deuterated compound [^{18}F]FECNT-d_4 may serve as a promising PET imaging agent to assess DAT-related disorders.

Key words: DAT, MicroPET imaging, ^{18}F, Deuterium, *In vivo* stability

Correspondence to: Zhengping Chen; *e-mail:* chenzhengping@jsinm.org

Published online: 13 April 2021

Introduction

The dopamine transporter (DAT) plays almost the sole executor of dopamine reutilization which is vitally correlated with Parkinson's disease (PD), and other neurodegenerative diseases [1, 2]. The dramatic loss of dopaminergic neurons in early-stage PD, found in previous clinicopathologic studies, suggests that the degeneration of this region begins before motor symptoms [3, 4]. As widely expressed in dopaminergic neurons, DAT is an important indicator for the diagnosis of early PD. Therefore, potential radioligands for image DAT with positron emission tomographic (PET) may aid diagnosis and treatment of PD by providing probes to estimate the density of DAT in specific brain regions.

Over the decades, researchers have developed several DAT radiotracers for PET imaging, ^{11}C-labelled ligands such as [^{11}C]PE2I [5] and [^{11}C]CFT [6]. However, ^{11}C has a very short half-life (20 min); ^{18}F-labelled ligands with a longer half-life (109 min) would be more practical for widespread use, such as [^{18}F]FP-CMT [7], [^{18}F]FE-PE2I [8], [^{18}F]LBT-999 [9], and [^{18}F]FECNT (2β-carbomethoxy-3β-(4-chlorophenyl)-8-(2-[^{18}F]fluoroethyl)nortropane) [10]. [^{18}F]FECNT has 25- and 156-fold selectivity for DAT (Ki = 1.5 nM) more than for serotonin transporter and noradrenaline transporter, respectively [10]. Davis et al. reported that PET imaging with [^{18}F]FECNT has favorable kinetics in humans and could distinguish DAT deficits between Parkinson's patients and healthy individuals [11]. However, it is found that [^{18}F]FECNT, which has the ^{18}F on the *N*-alkyl group, tends to be de-alkylated by cytochrome P450 enzyme to form radioactive metabolites, namely [^{18}F]fluoroacetaldehyde, [^{18}F]fluoroethanol, and [^{18}F]fluoroacetatic acid [12]. These metabolites can cross the blood-brain barrier (BBB) and distribute in the whole brain, confounding quantitative measurement of DAT. To accurately quantify the uptake and binding of [^{18}F]FECNT to DAT, Nye and colleagues raised an arterial input model of [^{18}F]FECNT uptake for DAT density quantification in humans [13]. However, this protocol required a 180-min PET scan and a series of arterial blood samples during imaging, which might be not convenient enough for clinical routine application. Nevertheless, this *N*-dealkylation metabolism pathway is not unique to [^{18}F]FECNT and has also been observed in other ligands with high affinity and selectivity for DAT such as [^{18}F]FE-PE2I [14] and [^{18}F]LBT-999 [15].

In recent years, a great deal of work has revealed the deuterium isotope effect on the biological reaction [16, 17]. Due to the cleavage rate of a carbon-deuterium (C–D) bond being about 6–7 times slower than that of a carbon-hydrogen (C–H) bond, the deuterium-substitution at easily metabolizable positions of the molecules can help to improve the metabolic stability of active pharmaceuticals [18, 19]. Recently, a deuterated form of tetrabenazine, SD-809, has been approved by the FDA to treat tardive dyskinesia [20]. Another example is CTP-656, a deuterated ivacaftor structure, which overcame many defects of the original drug such as short half-life and high clinical dosage [21]. Recently, the deuterium substitution strategy has also been applied to radiopharmaceutical for PET imaging. For example, [^{18}F]FE-(+)-DTBZ-d_4 [22] and [^{18}F]MNI-659-d_2 [23] were employed as radiotracers for vesicular monoamine transporter 2 (VMAT2) and phosphodiesterase 10A (PDE 10A), respectively.

In this study, we designed and synthesized a deuterated ^{18}F-labelled analogue [^{18}F]FECNT-d_4 (Fig. 1), aiming to improve upon the *in vivo* metabolic stability of [^{18}F]FECNT. Herein, we performed binding affinity, lipophilicity, autoradiography, biodistribution, and PET imaging of [^{18}F]FECNT-d_4. Our findings of excellent stability *in vivo* and high specific binding properties of [^{18}F]FECNT-d_4 imply that the deuterated tracer may be an attractive PET imaging agent for DAT.

Materials and Methods

General

All of the organic solvents and chemical reagents were obtained from Aladdin (China), J&K Scientific (China), Sigma-Aldrich (China), and used directly without further purification. FECNT and CFT were synthesized according to previously published papers [24, 25]. Kryptfix222 (K_{222}, 98.0 %) was purchased from ABX (Germany). Sep-Pak C18 cartridges and Sep-Pak lightweight QMA (QMA) were purchased from Waters (USA). Analytical high-performance liquid chromatography (HPLC) system was used to evaluate radiochemical purity (RCP) and the radiochemical yield (RCY) of [^{18}F]FECNT and [^{18}F]FECNT-d_4. Analytical high-performance liquid chromatography (HPLC) system consists of Waters 1525 HPLC pump, 2489 UV/Visible Detector (Waters, USA), and radiometric 610TR detector (PerkinElmer, USA). The analytical conditions were as follows: analytical column (C18, 5 μm, 4.6 × 150 mm, Phenomenex, Gemini, USA), 1.0 mL/min, UV detection at 220 nm, method A: H_2O/CH_3CN/Et_3N (40/60/0.1, v/v/v); method B: H_2O/CH_3CN/Et_3N (38/62/0.1, v/v/v). Semi-prepared HPLC (semi-prep HPLC) consists of Waters 1525 HPLC pump, 2489 UV/Visible Detector (Waters, USA), and flow-count radioactivity detector (Biscan, USA). The semi-prep HPLC system was used to separate and purify crude products. The preparation conditions (method C) were as follows: semi-prep column (C18, 5 μm, 10 × 250 mm, Waters, XBridge, USA), 5.0 mL/min, UV detection at 220 nm, H_2O/CH_3CN/Et_3N (45/55/0.1, v/v/v). The chemical structure of [^{18}F]FECNT-d_4 was identified by co-injected with the non-labelled standard compound.

The human neuroblastoma (SH-SY5Y) cell line was purchased from the National Collection of Authenticated Cell Cultures (Shanghai, China). The cells were cultured in DMEM: F12 medium (containing 1 % penicillin-

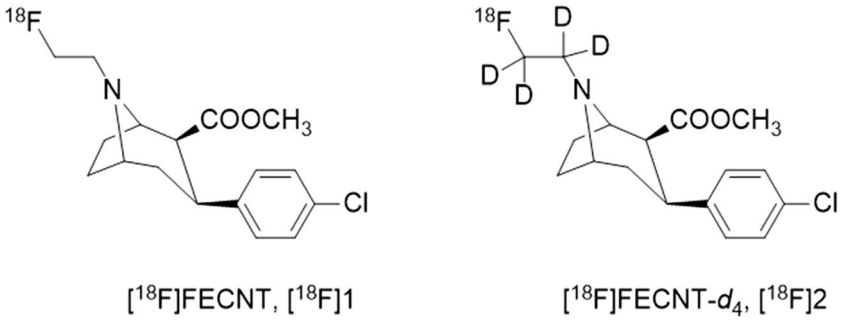

[18F]FECNT, [18F]1 [18F]FECNT-d_4, [18F]2

Fig. 1. Chemical structures of [18F]FECNT ([18F]1) and [18F]FECNT-d_4 ([18F]2).

streptomycin, 1 % gluta-max, 15 % fetal bovine serum) and kept under an atmosphere of 5 % CO_2 at 37 °C.

Male Sprague-Dawley (SD, 220−260 g) rats and Institute of Cancer Research mice (ICR, 20−30 g) were provided by Vital River Laboratory Animal Technology Co. Ltd. (China). The striatal unilateral 6-hydroxydopamine (6-OHDA) lesion model was performed with saline containing 16 μg (4 μg/μl) 6-OHDA, at the coordinates: AP: −4.0 mm (Bregma), ML: −1.4 mm (midline), DV: −7.5 mm (hole) [26]. All the animals were housed in clean cages with free access to food and water with a 12-h light-dark cycle and then tested. All animal experiment procedures were approved by the Animal Care and Ethics Committee of Jiangsu Institute of Nuclear Medicine.

Ethane-1,2-diyl-d_4 bis(4-Methylbenzenesulfonate) (4)

The compound (4) was synthesized following the procedures reported by Raaphorst et al. [27]. ^{1}H NMR (400 MHz, $CDCl_3$) δ 7.73 (d, J = 8.0 Hz, 4H), 7.33 (d, J = 8.0 Hz, 4H), 2.45 (s, 6H). ^{13}C NMR (100 MHz, $CDCl_3$) δ 145.40, 132.53, 130.10, 128.09, 66.12, 21.81. ESI-MS: m/z calcd for $C_{16}H_{14}D_4O_6S_2$ $[M+Na]^+$ 397.08, found 397.17.

2-Fluoroethyl-1,1,2,2-d_4 4-Methylbenzenesulfonate (5)

A solution of (4) (1.06 mmol, 1.0 equiv.) in acetonitrile (5 mL) was added to a solution of tetrabutylammonium fluoride (TBAF, 1.6 mmol, 1.5 equiv.) under nitrogen atmosphere. Then, the reaction system was heated to reflux for 1.5 h. The organic solvent was removed under reduced pressure and the residue was extracted with hexane/ethyl acetate (v/v = 5/1) and (5) was obtained as a colorless oil (101.3 mg, 43 %) after purification. ^{1}H NMR (400 MHz, $CDCl_3$) δ 7.84–7.77 (m, 2H), 7.40–7.32 (m, 2H), 2.45 (s, 3H). ^{13}C NMR (100 MHz, $CDCl_3$) δ 145.15, 132.69, 129.94, 127.96, 77.24, 29.70, 21.65. ESI-MS: m/z calcd for $C_9H_7D_4FO_3S$ $[M+Na]^+$ 245.07, found 245.13.

Methyl(1R,2S,3S,5S)-3-(4-Chlorophenyl)-8-(2-Hydroxyethyl-1,1,2,2-d_4)-8-Azabicyclo[3.2.1]Octane-2-Carboxylate (7)

Methyl(2*S*,3*S*)-3-(4-chlorophenyl)-8-azabicyclo[3.2.1]octane-2-carboxylate (6) (1 mmol, 1.0 equiv.), 2-bromoethan-1,1,2,2-d_4-1-ol (4 mmol, 4.0 equiv.), and triethylamine (5 mmol, 5.0 equiv.) were added to 3 mL of anhydrous acetonitrile. The solution was stirred at room temperature for 15 min to completely dissolve the solid. Subsequently, the reaction system was refluxed at 80 °C for 5 h. After the reaction was complete, the system turned yellow and the solvent was evaporated to dryness under reduced pressure. The residue was dissolved in dichloromethane and washed with 4 mL NaOH (1 M) and 4 mL water, respectively. The organic phase was dried over anhydrous Na_2SO_4 and filtered, and the filtrate was concentrated under reduced pressure. The residue was purified with silica gel chromatography with Et_2O/Et_3N (v/v = 95/5) to give (7) (279 mg, 85 %) as a white solid. ^{1}H NMR (400 MHz, $CDCl_3$) δ 7.24 (d, J = 8.6 Hz, 2H), 7.18 (d, J = 9.5 Hz, 2H), 3.60 (q, J = 3.8 Hz, 1H), 3.49 (s, 3H), 3.44–3.40 (m, 1H), 3.01 (dt, J = 12.7, 5.2 Hz, 1H), 2.92–2.88 (m, 1H), 2.60 (td, J = 12.7, 3.1 Hz, 1H), 2.14–1.95 (m, 2H), 1.82–1.74 (m, 1H), 1.74–1.66 (m, 2H), 1.64 (d, J = 11.8 Hz, 1H). ^{13}C NMR (100 MHz, $CDCl_3$) δ 172.23, 141.20, 131.93, 128.91, 128.27, 62.87, 61.09, 52.89, 51.43, 34.39, 34.21, 26.56, 26.22. ESI-MS: m/z calcd for $C_{17}H_{18}D_4ClNO_3$ $[M+H]^+$ 328.15, found 328.21.

Methyl(1R,2S,3S,5S)-3-(4-Chlorophenyl)-8-(2-((Methylsulfonyl)oxy)Ethyl-1,1,2,2-d_4)-8-Azabicyclo[3.2.1]Octane-2-Carboxylate (8)

A mixture of (7) (0.5 mmol, 1.0 equiv.) and methanesulfonic anhydride (2.2 mmol, 4.4 equiv.) in freshly dried dichloromethane (2 mL) was stirred at 30 °C for 3 days under nitrogen. The chemical purity of (8) was monitored by the analytical HPLC under the following condition (H_2O/CH_3CN/TFA, 65/35/0.2, v/v/v). After the reaction was complete, the solvent was removed under reduced pressure. The residue was dissolved in 1 mL dichloromethane and

washed with 2 mL ether 5 times. Finally, the precipitate was obtained by 99 % yield as a white solid (8) under reduced pressure. ^{1}H NMR (400 MHz, $CDCl_3$) δ 9.21 (s, 1H), 7.33–7.28 (m, 2H), 7.18–7.10 (m, 2H), 4.49 (d, J = 5.0 Hz, 2H), 3.44 (s, 4H), 3.21 (s, 3H), 3.05 (dd, J = 6.6, 2.3 Hz, 1H), 2.95 (t, J = 14.1 Hz, 1H), 2.84 (s, 3H), 2.71–2.49 (m, 2H), 2.18 (q, J = 11.0, 10.4 Hz, 2H), 2.04–1.95 (m, 1H). ^{13}C NMR (100 MHz, $CDCl_3$) δ 173.78, 136.36, 133.96, 129.14, 128.89, 64.31, 63.57, 52.96, 49.55, 39.55, 37.56, 34.08, 32.14, 24.79, 23.84. ESI-MS: m/z calcd for $C_{18}H_{20}D_4ClNO_5S$ $[M+H]^+$ 406.13, found 406.48.

2β-Carbomethoxy-3β-(4-Chlorophenyl)-8-(2-Fluoroethyl-1,1,2,2-d$_4$)-Nortropane (FECNT-d$_4$, 2)

A mixture of (6) (1 mmol, 1.0 equiv.), (5) (1 mmol, 1.0 equiv.), and *N*,*N*-diisopropylethylamine (DIPEA, 2 mmol, 2.0 equiv.) in methanol (8 mL) was heated at 100 °C for 24 h under nitrogen. After cooling to room temperature, the reaction mixture was stirred for 1 h with NaOH (1 M). Then the solution was concentrated with benzene under reduced pressure. The residue was purified by silica gel chromatography with PE/CH_2Cl_2 (4/1, v/v) to afford (2) as a white solid (128 mg, 38 %). ^{1}H NMR (400 MHz, $CDCl_3$) δ 7.25–7.21 (m, 2H), 7.21–7.16 (m, 2H), 3.78 (dd, J = 7.3, 3.5 Hz, 1H), 3.51 (s, 3H), 3.43 (q, J = 3.7 Hz, 1H), 2.97 (dt, J = 12.7, 5.0 Hz, 1H), 2.92–2.86 (m, 1H), 2.58 (td, J = 12.5, 2.9 Hz, 1H), 2.16–2.08 (m, 1H), 2.00 (td, J = 12.5, 8.0 Hz, 1H), 1.81–1.71 (m, 1H), 1.70–1.63 (m, 2H). ^{13}C NMR (100 MHz, $CDCl_3$) δ 171.73, 141.61, 131.49, 128.71, 128.00, 63.57, 62.22, 52.66, 51.05, 34.00, 33.61, 26.20, 25.77. ^{19}F NMR (376 MHz, $CDCl_3$) δ -222.10. MS calcd. for $C_{17}H_{17}D_4ClFNO_2$ $[M+H]^+$ 330.15, found: 330.42.

Radiosynthesis of [^{18}F]FECNT-d$_4$ ([^{18}F]2)

The synthetic method of [^{18}F]FECNT was referenced to the previous article [24]. The automatic radiosynthesis of [^{18}F]FECNT-d_4 was completed by the PET-MF-2 V-IT-1 (Beijing PET Technology, China) multifunctional synthesis module. First, [^{18}F]fluoride (10 GBq) was captured on the QMA cartridge by the enriched [^{18}O]H_2O through cyclotron. Then ^{18}F ion was transferred into the reaction tube from the irradiated QMA with a stock solution ((K_{222} (40 μmol), CH_3CN (0.8 mL), K_2CO_3 (20 μmol), water (0.2 mL)). The mixture was dried at 105 °C for 2 min under nitrogen, and further dried twice at 105 °C with ultra-dry acetonitrile. After drying, cool to 40 °C, the precursor (8) (5 mg) dissolved in CH_3CN (1 mL) was added to the reaction tube and kept at 90 °C for 20 min. Next, the reaction was quenched with H_2O (0.5 mL) and the mixture was transferred to the semi-prepared HPLC (method C). After purification, the collected liquid was diluted with 10-fold water and the tracer [^{18}F]FECNT-d_4 was trapped using a Sep-Pak C18 light cartridge. Then, the product was eluted with 1 mL of ethanol from the C18 cartridge. The product was analyzed for quality control by radio-HPLC (method A).

In vitro Stability Assays

The stability of [^{18}F]FECNT-d_4 was assayed in phosphate-buffered solution (PBS) and fetal bovine serum (FBS). [^{18}F]FECNT-d_4 (37 MBq) was added to PBS (pH 7.4, 500 μL) and FBS (500 μL), respectively. The mixtures were incubated for 0, 1, 2, 4, and 6 h at 37 °C. The radiochemical purity was recorded by analytical radio-HPLC (method A) at each time point. For serum samples, acetonitrile (100 μL) was added to a serum sample (100 μL) and the protein precipitate was removed by high-speed centrifugation before purity analysis.

In vivo Stability Assays

Following the injection of [^{18}F]FECNT-d_4 or [^{18}F]FECNT (20 MBq in 0.2 mL 10 % ethanol/saline) to the mice (n = 3), the blood samples were obtained from the mice's tail at 5, 30, and 60 min. Each sample was collected in a test tube containing CH_3CN (50 μL) with FECNT (20 μM). Male Sprague-Dawley rats (n = 3) were anesthetized with 2.5 % isoflurane in oxygen followed by intravenous injection of radioligand ([^{18}F]FECNT-d_4 or [^{18}F]FECNT: 185 MBq in 0.5 mL 10 % ethanol/saline). At 5, 30, and 60 min after injection, three rats were sacrificed at each time point respectively. The striatum and cerebellum were rapidly removed. Then, each sample of isolated striatum, cerebellum, and plasma was homogenized in 0.5 mL acetonitrile containing 1.0 mg/ml FECNT, respectively. The cold FECNT was added in samples to improve the extraction efficiency. The homogenates were centrifuged at 12,000g for 5 min at 4 °C for deproteinization. After centrifugation, the radioactivity counts of the supernatant and the precipitate were measured with a γ-counter (2480 Wizard^2, PerkinElmer, USA) separately to calculate the extraction efficiency of radioactive material. Finally, a portion of the resulting supernatant was injected into the analytical radio-HPLC system (method B). On the HPLC chromatogram, the percent ratio was calculated as the peak area of the unchanged form to total peak area (corrected for decay) × 100 %.

Cellular Uptake and Blocking Assays

SH-SY5Y cells were seeded into 12-well plates (1.5×10^5 cells per well) and cultured at 37 °C overnight for cell adherence. During the experiment, the cells were assigned for the control group, CFT blocking group, and DTBZ blocking group. The control group was added with [^{18}F]FECNT-d_4 (18.5 KBq) in fresh medium (200 μL), the other two groups were added with [^{18}F]FECNT-d_4 and CFT (20 μM) or [^{18}F]FECNT-d_4 and DTBZ (20 μM). The cells were separately incubated at 37 °C for 15, 30, 60, 90, and

120 min. At each time point, the basic medium was extracted to a test tube, and the cells were rinsed once with ice-cold PBS. Then, the cells were lysed and collected with NaOH (1 M) resolution. The radioactivity counts of cell lysate and supernatant were measured by a γ-counter and calculated as % uptake. The cellular uptake values of [^{18}F]FECNT-d_4 (mean ± SD, n = 3) were calculated as following formula: [CPM (the cell lysate)] / [CPM (the cell lysate) + CPM (the medium)] × 100 %. The blocking percentage was calculated with [CPM (control) − CPM (with inhibitor)] / CPM (control)] × 100 %.

Determination of Lipophilicity

The octanol-water partition coefficient of [^{18}F]FECNT-d_4 and [^{18}F]FECNT was determined at room temperature by the shake-flask method. [^{18}F]FECNT-d_4 or [^{18}F]FECNT (18.5 KBq) was added into two-phase mixture of *n*-octanol (3 mL) and PBS (pH 7.4, 3 mL). After shaking for 5 min, the PBS and the *n*-octanol phase were separated via centrifugation. Then, the PBS (1 mL) solution and *n*-octanol (1 mL) were pipetted into test tubes, respectively. The radioactivity in *n*-octanol and PBS were determined by a γ-counter. Subsequently, the remaining *n*-octanol (1 mL) was redistributed into a mixture containing 2 mL *n*-octanol and 3 mL PBS. The above experiment was repeated 5 times to obtain an average log*P* value. The log*P* values were calculated by the formula: $\log P = \log(\mathrm{CPM}_{n\text{-octanol}}/\mathrm{CPM}_{\mathrm{PBS}})$. All measurements were tested in triplicate.

Competitive Binding Assays

The rats were decapitated under ether anesthesia. The striatum (ST) was quickly pulled out and homogenized in 50 mM Tris-HCl buffer (pH 7.4) containing 120 mM NaCl, 2 mM KCl, 1 mM $CaCl_2$, and 1 mM $MgCl_2$ through a high throughput group grinder. Each 100 μL of homogenate is incubated with [^{18}F]FECNT (0.5–0.8 nM in buffer) and 100 μL of various concentrations of the test compound (FECNT-d_4 or FECNT, 10^{-11}–10^{-7} M) in a final volume of 0.5 mL of buffer. Non-specific binding was determined by co-incubation with 20 μM of CFT. These mixtures were incubated at room temperature for 30 min and terminated by rapid filtration using Whatman GF/C glass-fiber filters, followed by washing four times with ice-cold PBS. The radioactivity of the pellets bond with [^{18}F]FECNT was measured using an automatic γ-counter. The 50 % inhibitory concentration (IC_{50}) was calculated using the nonlinear least-square curve fitting with GraphPad Prism.

Biodistribution Studies

The rats were divided into 10 groups (n = 5) for the biodistribution studies. Each rat was injected with radioligand ([^{18}F]FECNT-d_4 or [^{18}F]FECNT: 12 MBq in 0.5 ml 10 % ethanol/saline) through the tail vein, and they were executed by cervical dislocation at 5, 15, 30, 60, and 120 min under anesthesia. The whole brain (including the striatum, cerebellum (CB), hippocampus (HIP), cortex (CX)) and each organ (including the heart, liver, spleen, lung, kidney, stomach, small intestines, testis, bone, muscle, pancreas) were quickly dissected and weighed. In addition, blood (200 μL) was obtained from the carotid artery. These radioactive samples were counted by a γ-counter and the results were expressed as a percentage of the injected dose per organ (% ID) or a percentage of the injected dose per gram of wet tissue (% ID/g) by calibrating with 1 % initial dose counts (100-fold diluted of the injection).

Ex vivo Autoradiography

Normal and 6-OHDA model rats were respectively injected with 37 MBq [^{18}F]FECNT-d_4 via the tail vein and sacrificed at 30 min post injection. The brain of each rat was separated and frozen quickly. Coronal sections (20 μm) were cut on a cryostat and dried at room temperature. The dried sections were exposed to the imager plate for 45 min, and images were attained using Cyclone Plus Storage Phosphor System (Perkin Elmer, USA).

MicroPET Imaging

A high-resolution microPET system (Siemens Medical Solutions, Knoxville, TN, Germany) was used to monitor 0–120 min scanning of the rat brain in real time. The rat was placed on the bed of microPET and the brain position was fixed under isoflurane anesthesia (2.5 % in oxygen gas) during the experiment. Each rat (n = 5) was injected with 12 MBq of [^{18}F]FECNT-d_4 or [^{18}F]FECNT (0.5 ml, 10 % ethanol/saline) through the tail vein. The scan results were acquired in 3 min per frame sequences to obtain 40 consecutive frames, and then images were reconstructed using the analytical filter back projection (FBP) method. Time activity curves (TACs) for tissue uptake were expressed as standard uptake values (SUVs). The injected radioactivity was corrected by time decay. To verify the specific binding of [^{18}F]FECNT-d_4 to DAT *in vivo*, a DAT-specific ligand CFT (1.0 mg/kg) was co-injected with [^{18}F]FECNT-d_4 into the tail vein and the rats were scanned from 10 to 40 min. Furthermore, the PD model rats were also scanned at 10–40 min after administration of [^{18}F]FECNT-d_4. All obtained images were processed and analyzed with ASIPro VM software; the regions of interest (ROIs) were plotted on summational images for a sum of all frames [28]. The binding potential (BP_{ND}) in the striatum was calculated by the simplified reference tissue method [29] using the TAC with the cerebellum as a reference region.

Results

Synthesis

The non-radioactive compound FECNT-d_4 was synthesized with (6) in 38 % yield. The mesylate precursor (8) was obtained in 99 % yield by esterification (Scheme 1). Finally, [^{18}F]FECNT-d_4 was synthesized from (8) by one step in a multifunctional synthesis module. The crude product solution was clear and colorless, and the RCP was greater than 99.9 % after purification. The molar activity (A_m) was 67 ± 12 GBq/μmol and the RCY was 46 ± 17 % (n = 15) at the end of [^{18}F]FECNT-d_4 synthesis.

In vitro Stability Assays

[^{18}F]FECNT-d_4 did not breakdown during its synthesis procedure. The HPLC analysis results showed satisfactory stability of [^{18}F]FECNT-d_4 for up to 6 h at 37 °C with RCP > 98 % in PBS and > 96 % in serum, respectively (Fig. 2).

In Vivo Stability Assays

To verify the *in vivo* stability of [^{18}F]FECNT-d_4 and [^{18}F]FECNT, it was necessary to analyze the parent tracer content in mice or rats after injected with radiotracer using radio-HPLC. The analysis showed that the retention times in the HPLC diagram were approximately 2.2 min for polar radioactive metabolites and 7.5 min for parent radiotracer. For mice, after administration of [^{18}F]FECNT-d_4 or [^{18}F]FECNT, polar metabolites of [^{18}F]FECNT began to appear in plasma at 30 min post administration. More metabolites of [^{18}F]FECNT were observed at 60 min, whereas only a little fraction of radiometabolites of [^{18}F]FECNT-d_4 were detected (Suppl. Fig. 1, see ESM). For rats, the parent tracer and radiolabelled metabolite fractions in brain tissues and plasma were described in Table 1.

Cellular Uptake and Blocking Assays

The cell uptake of [^{18}F]FECNT-d_4 was evaluated in SH-SY5Y cells. The accumulation of [^{18}F]FECNT-d_4 in SH-SY5Y cells reached 1.75 % uptake at 120 min. The binding specificity of [^{18}F]FECNT was preliminarily evaluated using CFT- and DTBZ-treated cells. Compared to the control group, the accumulation of [^{18}F]FECNT-d_4 was inhibited ~66 % (0.60 % uptake) by an excess of CFT at 120 min (Suppl. Fig. 2, see ESM). All the time, the uptake of [^{18}F]FECNT-d_4 was not influenced by DTBZ.

Lipophilicity and Binding Affinity

As shown in Table 2, the log$P_{7.4}$ values of [^{18}F]FECNT-d_4 and [^{18}F]FECNT were found to be 2.37 and 2.25, respectively. The IC_{50} values of the two compounds exhibited in

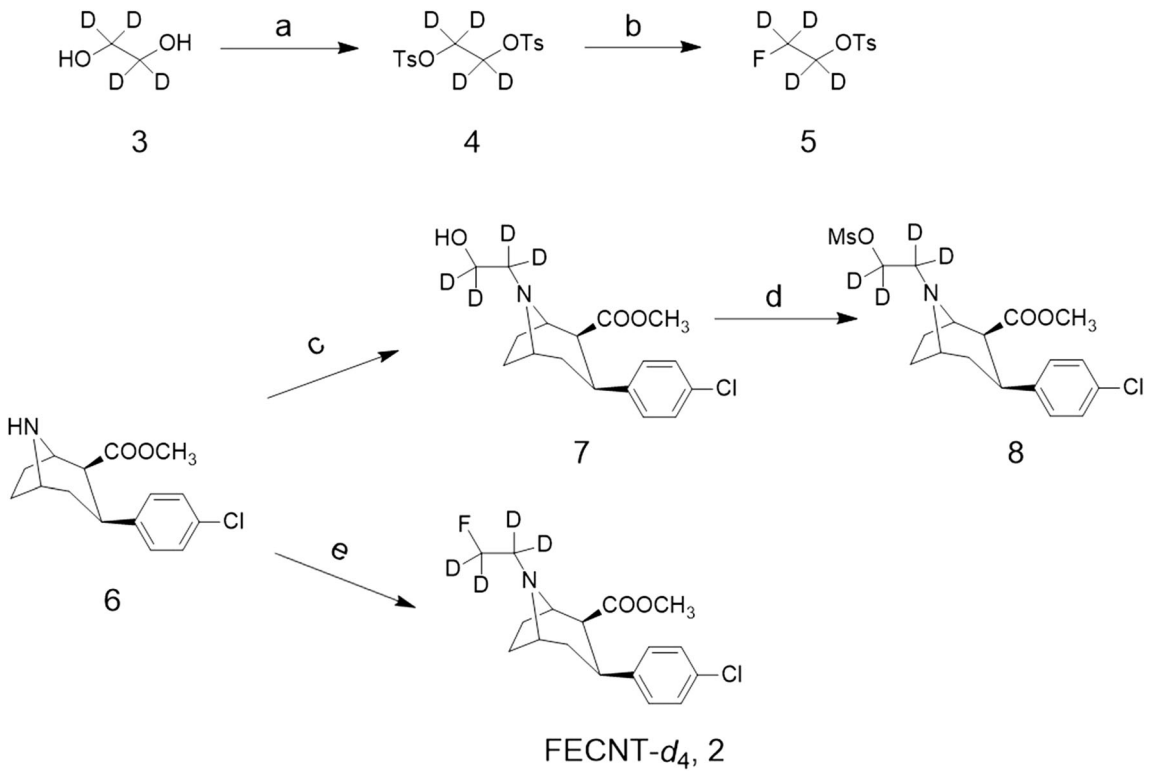

Scheme 1. Synthesis of FECNT-d_4 (2) and the precursor (8): (a) TsCl, rt, 24 h; (b) TBAF, CH_3CN, 80 °C; (c) $BrCD_2CD_2OH$, CH_3CN, 90 °C; (d) Ms_2O, CH_2Cl_2, 30 °C; (e) 5, DIPEA, CH_3OH, 100 °C.

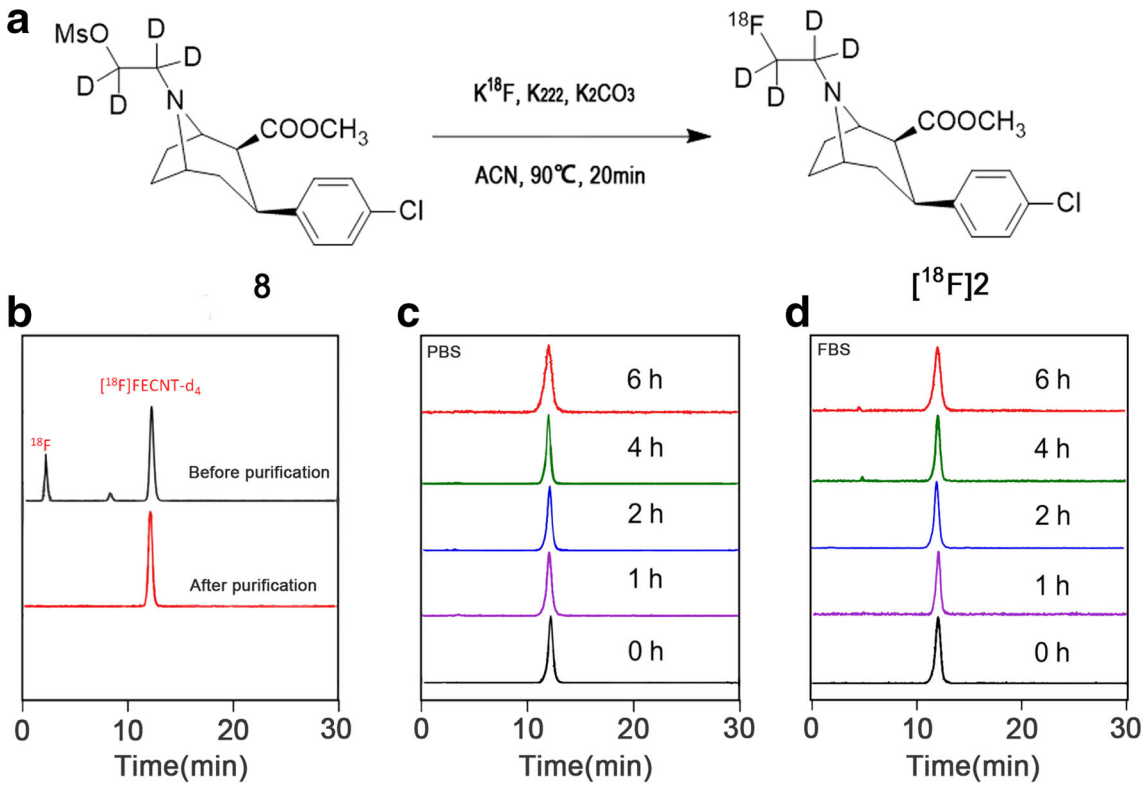

Fig. 2. **a** Radiolabelling of [^{18}F]FECNT-d_4 ([^{18}F]2) by one-step. **b** Radio-HPLC analysis of [^{18}F]FECNT-d_4 before and after purification. *In vitro* stability analysis of [^{18}F]FECNT-d_4 in PBS (**c**) or FBS (**d**) for different time (0, 1, 2, 4, 6 h).

the single-digit nanomolar range (FECNT-d_4, IC_{50} = 2.17 nM and FECNT, IC_{50} = 1.99 nM).

Biodistribution Studies

The biodistribution results of [^{18}F]FECNT-d_4 and [^{18}F]FECNT at each time point (5, 15, 30, 60, and 120 min) in rats were shown in Fig. 3. After the rats were severally injected with [^{18}F]FECNT-d_4 and [^{18}F]FECNT, the tracers were distributed primarily to the liver (15.81 ± 0.34 % ID vs 16.88 ± 1.46 % ID), lung (1.12 ± 0.17 % ID vs 1.93 ± 0.59 % ID), kidney (1.94 ± 0.08 % ID vs 1.82 ± 0.18 % ID), and brain (1.72 ± 0.10 % ID vs 1.66 ± 0.20 % ID), and lower accumulation in the bone, heart, small intestine, pancreas, and spleen. Brain distribution showed that the activity of [^{18}F]FECNT-d_4 in the striatum reached 2.03 ± 0.34 % ID/g at 5 min and retained at 2.06 ± 0.07 % ID/g until 30 min. The activity of [^{18}F]FECNT decreased rapidly in the striatum from 5 min (2.51 ± 0.28 % ID/g) to 30 min (1.58 ± 0.19 % ID/g).

Ex vivo Autoradiography

The regional distribution of [^{18}F]FECNT-d_4 in rat brain was further assessed by *ex vivo* autoradiography. As shown in Fig. 4, [^{18}F]FECNT-d_4 was located substantially in the caudate putamen (CPu), substantial nigra (SN), and nucleus accumbens (NAc), with low concentration in the cerebellum and cortex.

Table 1. Parent tracer and radiolabelled metabolite fractions in brain tissues and plasma of rats (% of total radioactivity, mean ± SD, n = 3)

	Time (min)	[^{18}F]FECNT-d_4			[^{18}F]FECNT		
		Striatum	Cerebellum	Plasma	Striatum	Cerebellum	Plasma
Parent tracer	5	98 ± 0.8 %	95 ± 3 %	76 ± 9 %	96 ± 2 %	89 ± 5 %	35 ± 15 %
	30	95 ± 2 %	77 ± 8 %	31 ± 7 %	82 ± 1 %	41 ± 9 %	16 ± 3 %
	60	91 ± 1 %	46 ± 8 %	13 ± 5 %	70 ± 4 %	27 ± 4 %	7 ± 1 %
Metabolites	5	2 ± 0.8 %	6 ± 3 %	24 ± 9 %	4 ± 2 %	11 ± 5 %	65 ± 15 %
	30	5 ± 2 %	23 ± 8 %	69 ± 7 %	18 ± 1 %	59 ± 9 %	84 ± 3 %
	60	9 ± 1 %	54 ± 8 %	87 ± 5 %	30 ± 4 %	73 ± 4 %	93 ± 1 %

Table 2. *In vitro* binding affinity and lipophilicity of compounds FECNT-d_4 and FECNT

Compound	IC_{50} (nM)	Log$P_{7.4}$
FECNT-d_4	2.17 (1.87–2.54)	2.37 (1.98–2.51)
FECNT	1.99 (1.70–2.34)	2.25 (2.12–2.39)

MicroPET Imaging

To confirm *in vivo* biological activity of [^{18}F]FECNT-d_4, microPET imaging was performed with normal and PD model rats. As shown in Fig. 5, in normal rats, prominent radioactivity was found in the striatum and the concentration could be inhibited to the background level by CFT. Meanwhile, in 6-OHDA unilaterally lesioned brains, the concentration of [^{18}F]FECNT-d_4 was noticeably reduced in the lesioned side relative to the unlesioned side. Dynamic TACs showed that the radioactivity of [^{18}F]FECNT-d_4 in the striatum maintained high uptake with SUVs of 4.02 ± 0.45 at 5–20 min, and the SUVs of [^{18}F]FECNT reached 4.11 ± 0.61 at 5 min and then declined rapidly. The volume of interest analysis by the Logan reference tissue method showed BP_{ND} of 1.95 ± 0.22 (mean ± SD, n = 5) for [^{18}F]FECNT-d_4 and 1.65 ± 0.51 (n = 5) for [^{18}F]FECNT, respectively.

Discussion

In this study, we synthesized [^{18}F]FECNT-d_4 as a PET ligand for DAT based on the chemical structure of FECNT. The novel agent [^{18}F]FECNT-d_4 presents a better target to non-target ratio and *in vivo* stability than the previously used contrast agent [^{18}F]FECNT. However, its application as a DAT radioligand in humans still needs further investigation. The present study provides the basis for future research.

To preliminarily assess [^{18}F]FECNT-d_4 bioactivity *in vitro*, we applied the radiotracer to the cellular uptake assay. The cellular uptake of [^{18}F]FECNT-d_4 showed a remarkable climbing tendency in 2 h, and the uptake of [^{18}F]FECNT-d_4 after pretreatment with the DAT inhibitor showed a 66 % tracer binding inhibition. However, the radioactivity did not decline when incubated with VMAT2 ligand. The results initially demonstrated its bioactivity and high selectivity for DAT (Suppl. Fig. 2, see ESM). Then, the binding affinity of FECNT-d_4 or FECNT to DAT was determined using [^{18}F]FECNT and rat striatum membrane homogenates. The results showed that FECNT-d_4 exhibited a comparable affinity for DAT to FECNT in the nanomolar range [10], which implied that binding affinity was almost unaffected by hydrogen-deuterium substitution.

Lipophilicity is one of the factors limiting a drug's ability to cross the BBB. In agreement with our hypothesis, the results of lipophilicity displayed that [^{18}F]FECNT-d_4 meets the criteria of appropriate log$P$ value ($2 < \log P < 3.5$) to cross the BBB [30]. This argument was also supported by the biodistribution of brain uptake. Biodistribution results showed that [^{18}F]FECNT-d_4 was rapidly distributed to the striatum but not retained in the regions without DAT. The ratio of target to non-target (ST/CB) at equilibrium can be used to evaluate specific binding in the target region of the brain. A comparative study of the biodistribution of [^{18}F]FECNT-d_4 and [^{18}F]FECNT in rats displayed that the two tracers have different brain metabolic trends (Fig. 3a, b). The ST to CB ratio of [^{18}F]FECNT-d_4 was higher than [^{18}F]FECNT at each point except at 5 min (Suppl. Table 2 and 4, see ESM). A slower elimination rate of [^{18}F]FECNT-d_4 than [^{18}F]FECNT was also found in other high uptake organs (Fig. 3c, d). These results indicated that [^{18}F]FECNT-d_4 improved the ratio of target to non-target and decelerated the drug's degradation rate *in vivo* compared to [^{18}F]FECNT. Besides, we found that the bone uptakes in biodistribution results were very low from 0 to 120 min for both [^{18}F]FECNT-d_4 and [^{18}F]FECNT, suggesting the stability of [^{18}F]fluoroethyl group with negligible *in vivo* defluorination [18, 31].

Then, the specific binding of [^{18}F]FECNT-d_4 to DAT *in vivo* was confirmed using *ex vivo* autoradiography and microPET imaging. Autoradiography in normal rats showed high accumulation of [^{18}F]FECNT-d_4 in the CPu, NAc, and SN, with abundant radioactivity in the symmetrical striata and low uptake in the CB and cortex. The binding specificity of [^{18}F]FECNT-d_4 was confirmed to be consistent with the known localization of DAT in rodent brains [32]. Besides, in unilateral PD model rats, an obvious reduction of [^{18}F]FECNT-d_4 uptake was found in the lesioned hemisphere relative to the unlesioned side (Fig. 4).

MicroPET imaging was performed on normal and PD model rats to further evaluate the potential of [^{18}F]FECNT-d_4 for DAT tracing (Fig. 5a). The resulting images were well aligned with autoradiography which showed high tracer uptake in regions of DAT-rich striata. The sufficient brain uptake and rapid washout of non-target tissue of the tracer showed in dynamic TAC were in agreement with biodistribution results of brain tissue. The uptake of [^{18}F]FECNT-d_4 in the striatum remained a relatively stable high-plateau period at 5–20 min, whereas the uptake of [^{18}F]FECNT in the striatum began to decrease from 4 min after injection (Fig. 5b). While co-injected with the well-characterized specific DAT ligand, the uptake of [^{18}F]FECNT-d_4 was mostly inhibited in the target, resulting in the target to non-target ratio close to unity (ST/CB = 1.04). The BP_{ND} values of both radioligands were 1.95 ± 0.22 for [^{18}F]FECNT-d_4 and 1.65 ± 0.51 for [^{18}F]FECNT. The results indicated that the binding potential of [^{18}F]FECNT-d_4 in the rat striatum was higher and more stable than that of [^{18}F]FECNT. The binding potential of [^{18}F]FECNT-d_4 in rat striatum was comparable to that of another DAT imaging agent, [^{18}F]FP-CMT (2.50 ± 0.25) [7]. A radiopharmaceutical of another tropane analogue, [^{18}F]LBT999, has a significantly higher BP_{ND} (4.39 ± 0.31)

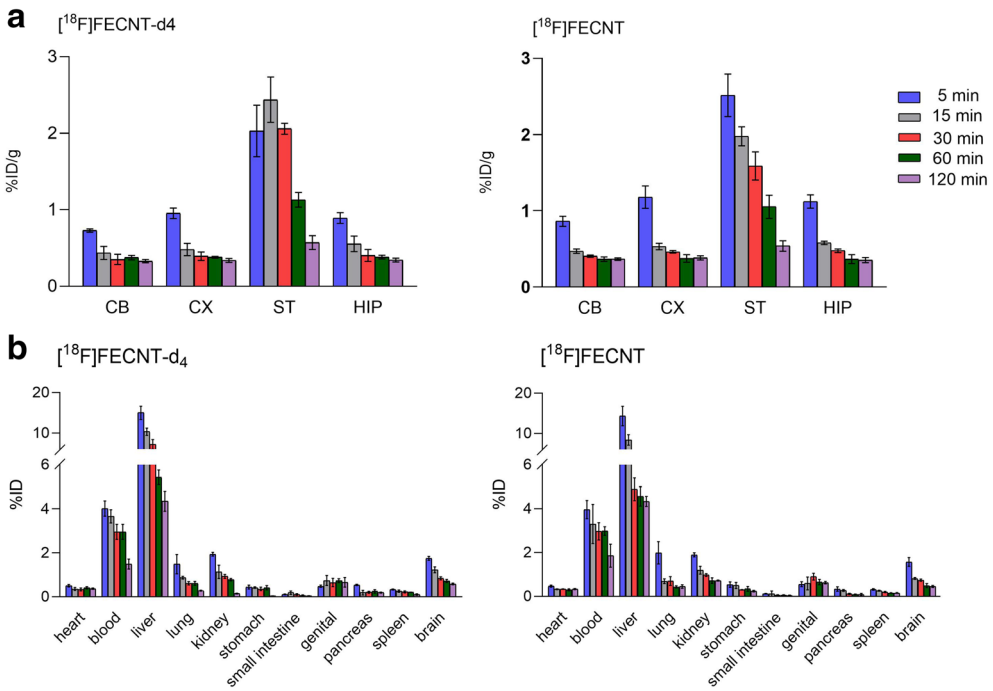

Fig. 3. Biodistribution of [^{18}F]FECNT-d_4 and [^{18}F]FECNT in rats. **a** Brain data of [^{18}F]FECNT-d_4 and [^{18}F]FECNT were expressed as the percentage of injected dose per gram of tissue (% ID/g, n = 5, mean ± SD). **b** Organ data of [^{18}F]FECNT-d_4 and [^{18}F]FECNT were expressed as the percentage of the injected dose per organ (% ID, n = 5, mean ± SD).

in rats [33] and investigated in patients with dopaminergic impairment [34, 35]. However, the effects of metabolites on BP_{ND} during prolonged scanning (4 h) are appreciable [36]. Although the binding potential was lower than some of other DAT tracers, [^{18}F]FECNT-d_4 still showed good brain uptake and target to non-target ratio, allowing good visualization of DAT in striatal and extra-striatal regions.

After *in vitro* and *in vivo* biological studies, we analyzed the metabolism of [^{18}F]FECNT-d_4 *in vivo*. A competent radiotracer should be stable *in vivo* to retain its biological activity. Similar to cocaine [37], the tropane derivatives would undergo oxidative cleavage of the *N*-substituent and other metabolic pathways *in vivo*. For tropane analogues, CYP3A4 exhibited the highest catalytic activity for *N*-dealkylation [38]. Indeed, *in vivo* stability studies in rats showed that [^{18}F]FECNT-d_4 also transformed to polar metabolite. The major metabolite was issued from *N*-dealkylation, concomitantly with the departure of the fluoroalkyl chain (formation of fluorine ethanol or its oxidation product). Thirty minutes after the injection, around 69 % of the parent [^{18}F]FECNT-d_4 in plasma was transformed, and such polar metabolites of [^{18}F]FECNT have been demonstrated in human and non-human primate plasma [12]. Nevertheless, the metabolic results showed that the parent fraction of [^{18}F]FECNT-d_4 in striatum (91 %) was predominant up to 60 min post injection. At 30 min, there were only 16 % of the unchanged [^{18}F]FECNT in plasma and 82 % in striatum. The metabolic stability of

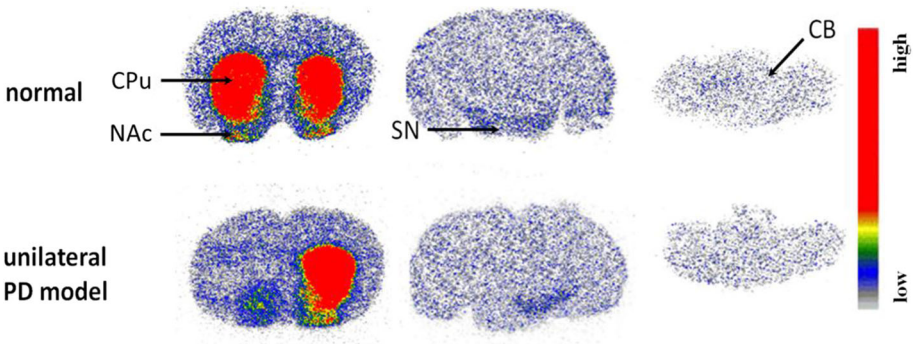

Fig. 4. Representative *ex vivo* autoradiography of DAT binding sites in normal or PD model rats' brains. The intensity of [^{18}F]FECNT-d_4 binding was well matched with the DAT expression in the brain. CPu, caudate putamen; NAc, nucleus accumbens; SN, substantia nigra; CB, cerebellum.

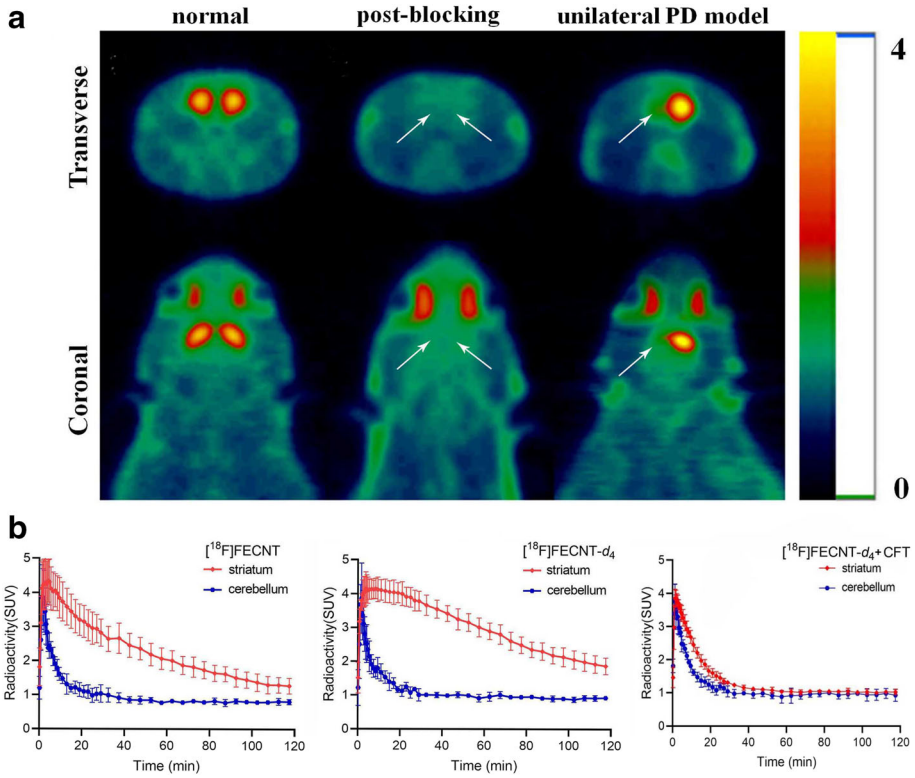

Fig. 5. **a** Representative PET images of [^{18}F]FECNT-d_4 in brains of rats. Each PET image was generated by the summation of data collected 10–40 min after injection. The white arrows indicate the striatum. **b** TACs of [^{18}F]FECNT-d_4 and [^{18}F]FECNT were obtained from regions of interest located on the striatum and cerebellum during 0–120 min and the TACs of [^{18}F]FECNT-d_4 were blocked by DAT ligand CFT. Values were generated at fixed times after injection during PET scan and shown as mean ± SD, n = 5.

[^{18}F]FECNT-d_4 observed in rats was superior to that of [^{18}F]FECNT. Interestingly, we also found a more *in vivo* stability of the tracers in mice than in rats, probably due to the different kinetics of drug metabolism between the species.

Some other ^{18}F-labelled tropane analogs targeting DAT, such as [^{18}F]FP-CMT, [^{18}F]FE-PE2I and [^{18}F]LBP999, have been reported and their in vivo metabolism have been investigated. Metabolite analysis of [^{18}F]FP-CMT produced only one hydrophilic polar metabolite *in vivo* [7]. The longer carbon chain at the *N*-substituent seems to produce less oxidative dealkylation *in vivo* [39]. However, the metabolic analysis in rats displayed that [^{18}F]FP-CMT has a fast metabolic rate with ~88 % parent molecule transformed at 30 min post injection [7]. The polar metabolite was supposed to be a 4-carboxy analogue of [^{18}F]FP-CMT, but the metabolite's brain penetration ability was not be ascertained. Besides *N*-dealkylation, [^{18}F]FE-PE2I also suffers from hydroxylation and benzylic hydroxylation to yield a series of brain-penetrating metabolites [40]. The *in vivo* metabolism rate of [^{18}F]FE-PE2I appears rapid kinetics in humans, with 86 % of the parent molecule transformed at 30 min post injection [41]. The prominent accumulation of major radiometabolite 4-hydroxymethyl analogue in the striatum suggests a high affinity for DAT as well as 4-carboxy analogue presents non-specific binding in the brain [41]. These results might confound the quantitative analysis. The radiopharmaceutical of the same chemical class, [^{18}F]LBT999, appears more stable with a slow transformation rate *in vivo*. There was 60 % unmetabolized plasmatic fraction in humans at 30 min post injection [35], which seems to facilitate clinical imaging. However, the ligand [^{18}F]LBT999 has the same behavior as the biotransformation of PE2I, suggesting that its metabolites also affect PET images and subsequent quantification [42]. Furthermore, the high bone accumulation of the radioactivity implicated high defluorination of [^{18}F]LBT999 [15]. In recent years, in order to overcome these limitations, great efforts have been made to search for better DAT imaging agents. Although the tropane derivative still undergoes metabolism after deuterium substitution, the present study showed that replacing the *N*-fluoroethyl group of [^{18}F]FECNT with an *N*-fluoroethyl-d_4 could reduce the oxidative cleavage of the *N*-substituent and led to a significant improvement in the pharmacological profile of this ligand.

Conclusion

In summary, we prepared and characterized a novel deuterated compound [^{18}F]FECNT-d_4 based on the tropane structure which was confirmed as a good candidate for DAT

imaging. As demonstrated by microPET imaging, in conjunction with biodistribution assays and plasma metabolism studies, [^{18}F]FECNT-d_4 displayed a combination of superior brain uptake and better *in vivo* stability in rats. These results indicate that the ^{18}F-labelled FECNT-d_4 tracer is applicable for neuroimaging and worthy of further clinical investigations.

Supplementary Information. The online version contains supplementary material available at https://doi.org/10.1007/s11307-021-01603-2.

Funding. This work was supported by the National Natural Science Foundation of China (81671723, 81801742), the Natural Science Foundation of Jiangsu Province (BK20201133), Wuxi Municipal Science and Technology Development Fund (WX18IIAN048, N20192015), Program from Jiangsu Commission of Health (H2018086), and Wuxi Municipal Health Commission (Q201946).

Declarations

Conflict of Interest

The authors declare that they have no conflict of interest.

References

1. Marshall V, Grosset D (2003) Role of dopamine transporter imaging in routine clinical practice. Mov Disord 18:1415–1423
2. McHugh PC, Buckley DA (2015) The structure and function of the dopamine transporter and its role in CNS diseases. Vitam Horm 98:339–369
3. Dauer W, Przedborski S (2003) Parkinson's disease: mechanisms and models. Neuron 39:889–909
4. Poewe W, Seppi K, Tanner CM, Halliday GM, Brundin P, Volkmann J, Schrag AE, Lang AE (2017) Parkinson disease. Nat Rev Dis Primers 3:17013
5. Halldin C, Erixon-Lindroth N, Pauli S, Chou YH, Okubo Y, Karlsson P, Lundkvist C, Olsson H, Guilloteau D, Emond P, Farde L (2003) [^{11}C]PE2I: a highly selective radioligand for PET examination of the dopamine transporter in monkey and human brain. Eur J Nucl Med Mol Imaging 30:1220–1230
6. Hantraye P, Brownell A, Elmaleh D, Spealman RD, Wullner U, Brownell GL, Madras BK, Isacson O (1992) Dopamine fiber detection by [^{11}C]-CFT and PET in a primate model of parkinsonism. Neuroreport 3:265–268
7. Cumming P, Maschauer S, Riss PJ, Tschammer N, Fehler SK, Heinrich MR, Kuwert T, Prante O (2014) Radiosynthesis and validation of [^{18}F]FP-CMT, a phenyltropane with superior properties for imaging the dopamine transporter in living brain. J Cereb Blood Flow Metab 34:1148–1156
8. Suzuki M, Ito H, Kodaka F, Takano H, Kimura Y, Fujiwara H, Sasaki T, Takahata K, Nogami T, Nagashima T, Nengaki N, Kawamura K, Zhang MR, Varrone A, Halldin C, Okubo Y, Suhara T (2014) Reproducibility of PET measurement for presynaptic dopaminergic functions using L-[beta-[^{11}C]DOPA and [^{18}F]FE-PE2I in humans. Nucl Med Commun 35:231–237
9. Chalon S, Hall H, Saba W, Garreau L, Dollé F, Halldin C, Emond P, Bottlaender M, Deloye JB, Helfenbein J, Madelmont JC, Bodard S, Mincheva Z, Besnard JC, Guilloteau D (2006) Pharmacological characterization of (E)-N-(4-fluorobut-2-enyl)-2beta-carbomethoxy-3beta-(4'-tolyl)nortropane (LBT-999) as a highly promising fluorinated ligand for the dopamine transporter. J Pharmacol Exp Ther 317:147–152
10. Goodman MM, Kilts CD, Keil R, Shi B, Martarello L, Xing D, Votaw J, Ely TD, Lambert P, Owens MJ, Camp VM, Malveaux E, Hoffman JM (2000) ^{18}F-Labeled FECNT: a selective radioligand for PET imaging of brain dopamine transporters. Nucl Med Biol 27:1–12
11. Davis MR, Votaw JR, Bremner JD, Byas-Smith MG, Faber TL, Voll RJ, Hoffman JM, Grafton ST, Kilts CD, Goodman MM (2003) Initial human PET imaging studies with the dopamine transporter ligand ^{18}F-FECNT. J Nucl Med 44:855–861
12. Zoghbi SS, Shetty HU, Ichise M, Fujita M, Imaizumi M, Liow JS, Shah J, Musachio JL, Pike VW, Innis RB (2006) PET imaging of the dopamine transporter with ^{18}F-FECNT: a polar radiometabolite confounds brain radioligand measurements. J Nucl Med 47:520–527
13. Nye JA, Votaw JR, Bremner JD, Davis MR, Voll RJ, Camp VM, Goodman MM (2014) Quantification of dopamine transporter density with [^{18}F]FECNT PET in healthy humans. Nucl Med Biol 41:217–222
14. Varrone A, Steiger C, Schou M, Takano A, Finnema SJ, Guilloteau D, Gulyás B, Halldin C (2009) In vitro autoradiography and in vivo evaluation in cynomolgus monkey of [^{18}F]FE-PE2I, a new dopamine transporter PET radioligand. Synapse 63:871–880
15. Peyronneau MA, Saba W, Dolle F, Goutal S, Coulon C, Bottlaender M, Valette H (2012) Difficulties in dopamine transporter radioligand PET analysis: the example of LBT-999 using [^{18}F] and [^{11}C] labelling: part II: Metabolism studies. Nucl Med Biol 39:347–359
16. Parcella K, Eastman K, Yeung KS, Grant-Young KA, Zhu J, Wang T, Zhang Z, Yin Z, Parker D, Mosure K, Fang H, Wang YK, Lemm J, Zhuo X, Hanumegowda U, Liu M, Rigat K, Donoso M, Tuttle M, Zvyaga T, Haarhoff Z, Meanwell NA, Soars MG, Roberts SB, Kadow JF (2017) Improving metabolic stability with deuterium: the discovery of BMT-052, a pan-genotypic HCV NS5B polymerase inhibitor. ACS Med Chem Lett 8:771–774
17. Roston D, Islam Z, Kohen A (2013) Isotope effects as probes for enzyme catalyzed hydrogen-transfer reactions. Molecules 18:5543–5567
18. Kuchar M, Mamat C (2015) Methods to increase the metabolic stability of ^{18}F-radiotracers. Molecules 20:16186–16220
19. Pirali T, Serafini M, Cargnin S, Genazzani AA (2019) Applications of deuterium in medicinal chemistry. J Med Chem 62:5276–5297
20. Schmidt C (2017) First deuterated drug approved. Nat Biotechnol 35:493−494
21. Harbeson SL, Morgan AJ, Liu JF, Aslanian AM, Nguyen S, Bridson GW, Brummel CL, Wu L, Tung RD, Pilja L, Braman V, Uttamsingh V (2017) Altering metabolic profiles of drugs by precision deuteration 2: discovery of a deuterated analog of ivacaftor with differentiated pharmacokinetics for clinical development. J Pharmacol Exp Ther 362:359–367
22. Jahan M, Eriksson O, Johnström P, Korsgren O, Sundin A, Johansson L, Halldin C (2011) Decreased defluorination using the novel betacell imaging agent [^{18}F]FE-DTBZ-d_4 in pigs examined by PET. EJNMMI Res 1:1–13
23. Mori W, Yamasaki T, Fujinaga M, Ogawa M, Zhang Y, Hatori A, Xie L, Kumata K, Wakizaka H, Kurihara Y, Ohkubo T, Nengaki N, Zhang MR (2019) Development of 2-(2-(3-(4-([^{18}F]Fluoromethoxy- d_2)phenyl)-7-methyl-4-oxo-3,4-dihydroquinazolin-2-yl)ethyl)-4-isopropoxyisoindoline-1,3-dione for positron-emission-tomography imaging of phosphodiesterase 10A in the brain. J Med Chem 62:688–698
24. Chen ZP, Wang SP, Li XM, Liu CY, Tang J, Cao GX, Luo SN, Zhang LF, Jin J (2008) A one-step automated high-radiochemical-yield synthesis of [^{18}F]FECNT from mesylate precursor. Appl Radiat Isot 66:1881–1885
25. Xu L, Trudell ML (1996) Stereoselective synthesis of 2beta-carbomethoxy-3beta-phenyltropane derivatives. J Heterocyclic Chem 33:2037–2039
26. Tang J, Xu Y, Liu C, Fang Y, Cao S, Zhao C, Huang H, Zou M, Chen Z (2020) PET imaging with [^{18}F]FP-(+)-DTBZ in 6-OHDA-induced partial and full unilaterally-lesioned model rats of Parkinson's disease and the correlations to the biological data. Nucl Med Biol 90-91:1–9
27. Raaphorst RM, Luurtsema G, Schokker CJ, Attia KA, Schuit RC, Elsinga PH, Lammertsma AA, Windhorst AD (2018) Improving metabolic stability of fluorine-18 labeled verapamil analogs. Nucl Med Biol 64-65:47–56
28. Sun Y, Liu C, Chen Z, Li B, Lv Z, Wang J, Lou J, Tang J, Wang Y, Zhang G, Liu X (2020) A phase 2, open-label, multi-center study to evaluate the efficacy and safety of ^{99m}Tc-TRODAT-1 SPECT to detect Parkinson's disease. Ann Nucl Med 34:31–37
29. Lammertsma AA, Hume SP (1996) Simplified reference tissue model for PET receptor studies. Neuroimage 4:153–158

30. Waterhouse RN (2003) Determination of lipophilicity and its use as a predictor of blood–brain barrier penetration of molecular imaging agents. Mol Imaging Biol 5:376–389
31. Pan J, Pourghiasian M, Hundal N, Lau J, Bénard F, Dedhar S, Lin KS (2013) 2-[^{18}F]fluoroethanol and 3-[^{18}F]fluoropropanol: facile preparation, biodistribution in mice, and their application as nucleophiles in the synthesis of [^{18}F]fluoroalkyl aryl ester and ether PET tracers. Nucl Med Biol 40:850–857
32. Cumming P, Maschauer S, Riss PJ, Grill E, Pischetsrieder M, Kuwert T, Prante O (2015) Perturbed development of striatal dopamine transporters in fatty versus lean Zucker rats: a follow-up small animal PET study. Mol Imaging Biol 17:521–528
33. Serriere S, Tauber C, Vercouillie J, Guilloteau D, Deloye J, Garreau L, Galineau L, Chalon S (2014) In vivo PET quantification of the dopamine transporter in rat brain with [^{18}F]LBT-999. Nucl Med Biol 41:106–113
34. Ribeiro MJ, Vercouillie J, Arlicot N, Tauber C, Gissot V, Mondon K, Barantin L, Cottier JP, Maia S, Deloye JB, Emond P, Guilloteau D (2020) Usefulness of PET With [^{18}F]LBT-999 for the evaluation of presynaptic dopaminergic neuronal loss in a clinical environment. Front Neurol 11:754
35. Arlicot N, Vercouillie J, Malherbe C, Bidault R, Gissot V, Maia S, Barantin L, Cottier J, Deloye J, Guilloteau D, Ribeiro M (2019) PET imaging of dopamine transporter with [^{18}F]LBT-999: initial evaluation in healthy volunteers. Q J Nucl Med Mol Imaging. https://doi.org/https://doi.org/10.23736/S1824-4785.19.03175-3
36. Varrone A, Stepanov V, Nakao R, Toth M, Gulyas B, Emond P, Deloye JB, Vercouillie J, Stabin MG, Jonsson C, Guilloteau D, Halldin C (2011) Imaging of the striatal and extrastriatal dopamine transporter with [^{18}F]LBT-999: quantification, biodistribution, and radiation dosimetry in nonhuman primates. J Nucl Med 52:1313–1321
37. Kloss MW, Rosen GM, Rauckman EJ (1983) N-demethylation of cocaine to norcocaine: evidence for participation by cytochrome P-450 and FAD-containing monooxygenase. Mol Pharmacol 23:482–485
38. Couth RT, Su P, Baker GB (1994) Involvement of CYP2D6, CYP3A4, and other cytochrome P-450 isozymes in N-dealkylation reactions. J Pharmacol Toxicol Methods 4:177–186
39. Gu X-H, Zong R, Kula NS, Baldessarinib RJ, Neumeyer JL (2001) Synthesis and biological evaluation of a series of novel N- or O-fluoroalkyl derivatives of tropane: potential positron emission tomography (PET) imaging agents for the dopamine transporter. Bioorg Med Chem Lett 1123:3049–3053
40. Amini N, Nakao R, Schou M, Halldin C (2013) Identification of PET radiometabolites by cytochrome P450, UHPLC/Q-ToF-MS and fast radio-LC: applied to the PET radioligands [^{11}C]flumazenil, [^{18}F]FE-PE2I, and [^{11}C]PBR28. Anal Bioanal Chem 405:1303–1310
41. Sasaki T, Ito H, Kimura Y, Arakawa R, Takano H, Seki C, Kodaka F, Fujie S, Takahata K, Nogami T, Suzuki M, Fujiwara H, Takahashi H, Nakao R, Fukumura T, Varrone A, Halldin C, Nishikawa T, Suhara T (2012) Quantification of dopamine transporter in human brain using PET with [^{18}F]FE-PE2I. J Nucl Med 53:1065–1073
42. Malherbe C, Bidault R, Netter C, Guilloteau D, Vercouillie J, Arlicot N (2019) Development of a fast and facile analytical approach to quantify radiometabolites in human plasma samples using ultra high-performance liquid chromatography. Am J Anal Chem 10:185–201